JOURNAL OF MATERIALS SCIENCE 28 (1993) 4442–4450

Yield and fracture behaviour of cross-linked epoxies

U. M. VAKIL*, G. C. MARTIN
Department of Chemical Engineering and Materials Science, Syracuse University, Syracuse, NY 13244, USA

The yield stress and fracture energies of a series of cross-linked epoxy resins were studied in order to correlate the macroscopic mechanical properties with the polymer microstructure. Five networks with varying cross-link densities were synthesized by reacting a homologous series of epoxy resins with stoichiometric quantities of *m*-phenylenediamine. For all the networks, the yield stress decreased with increasing temperatures in accordance with the predictions of the Eyring theory of viscosity. At constant temperatures, the yield stress decreased with increasing molecular weight between cross-links. The fracture studies revealed two distinct types of crack propagation behaviour above and below approximately 0 °C. Below 0 °C the cracks propagated in a stable and continuous manner, while the crack propagation behaviour changed to an unstable "stick–slip" mode as the test temperature was increased above 0 °C. For unstable crack growth, the fracture energies for crack initiation increased with increasing temperature, while the fracture energies for crack arrest were, within the limits of experimental error, independent of temperature. The crack arrest fracture energies were similar in magnitude to the fracture energies for stable crack propagation. An empirical power-law type correlation was observed between the glassy arrest fracture energies and the average molecular weight between cross-links. Micrographs of specimens which failed by the unstable, "stick–slip" mode revealed characteristic plastic deformation zones which highlighted the positions of crack initiation and arrest along the crack path. The deformation zone widths were observed to increase with increasing test temperatures, providing evidence of greater localized plastic deformations and higher fracture initiation energies at higher temperatures.

1. Introduction

Polymer resins are used extensively in structural, load-bearing applications in the aerospace, automotive, and marine industries. For these applications, the resins are used either as adhesives or as matrices in fibre-reinforced composites. While thermoplastic resins have gained limited use in composite manufacture, the resins most extensively used thus far are cross-linked thermosets. Amongst the variety of thermosets, epoxies enjoy the most widespread use and their curing chemistry is also most extensively studied.

At room temperature, cross-linked epoxies typically exhibit high moduli and near elastic stress–strain behaviour but they have poor resistance to fracture. Several techniques, such as the addition of rubber modifiers and rigid particles, have been used to improve the fracture strength of cross-linked epoxies. However, the fundamental relationship between the polymer microstructure and its fracture behaviour is still not adequately understood.

The objectives of this research were to determine the mechanical properties of a series of cross-linked resins with well-defined structures and to analyse the influence of the network structure on the fracture behaviour. The networks were characterized in terms of the average molecular weights between cross-links. The cure conditions and physical properties of the networks are described elsewhere [1]. The temperature and the molecular weight dependence of the yield stress and the fracture energies, and the effects of localized yielding on fracture mechanisms are discussed here.

2. Experimental procedure

2.1. Materials

The structure of the epoxy resins is shown in Fig.1 and the resin characteristics are listed in Table I. The resins are designated Epon 825, 836, 1001F, 1002F and 1004F, according to the manufacturer's nomenclature. All resins were obtained from the Shell Chemical Co., and were used without further purification. Each resin was cross-linked with stoichiometric quantities of *m*-phenylenediamine (*m*PDA) to form the networks [1]. Stoichiometric compositions and initial cure temperatures less than 150 °C were chosen to induce network formation via the epoxy–amine addition reactions, by limiting the extent of the etherification reaction and to

**Present address*: AdTech Systems Research Inc., 1342 North Fairfield Road, Dayton, OH 45432, USA.

0022–2461 © *1993 Chapman & Hall*

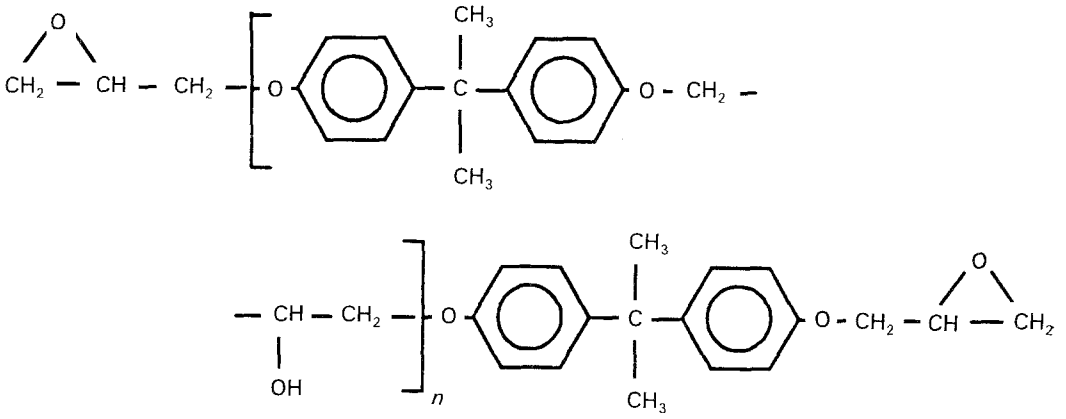

Figure 1 Structure of Epon resins

TABLE I Physical properties of epoxy resins

Resin	Equivalent weight (g/eq)	Average value of n[a]	Melting point (°C)
Epon 825	175.0	0.04	42.3
Epon 836	314.8	1.02	12.6
Epon 1001F	544.9	2.64	42.8
Epon 1002F	648.5	3.37	49.3
Epon 1004F	833.4	4.67	60.2

[a] n is defined in Fig. 1.

TABLE II Molecular weight between cross-links for fully cured networks

Network	$\bar{M}_c$ [1] (g mol^{-1})
Epon 825/*m*PDA	257.3
Epon 836/*m*PDA	527.0
Epon 1001F/*m*PDA	774.4
Epon 1002F/*m*PDA	1042.9
Epon 1001F/*m*PDA	1286.2

thereby yield "near ideal" networks with epoxy chains end-linked by the amine molecules.

In addition to Epon 825, 836, 1001F, 1002F and 1004F, two blends were prepared by mixing different quantities of the base Epon resins such that the equivalent weight of the resulting blend was identical to that of one of the base resins; i.e. a blend with an epoxy equivalent weight equal to that of Epon 1001F was made by mixing appropriate quantities of Epon 825 and Epon 1004F, and a blend with an equivalent weight equal to Epon 836 was made by blending Epon 825 and Epon 1001F. For the epoxy/amine ratio and the cure schedules, the blends were treated as having the properties of the base resins with the same equivalent weights. The blends are designated Blend (836) and Blend (1001).

The network conversions and the ultimate glass transition temperatures were determined by Fourier transform infrared spectroscopy and differential scanning calorimetry. The average molecular weights between cross-links of the fully reacted networks were calculated from the dynamic mechanical shear moduli and also from the reaction stoichiometry [1]. The $\bar{M}_c$ values are listed in Table II.

2.2. Yield stress

For highly cross-linked polymers such as the epoxies used in this study, the tensile stress is often greater than the uniaxial tensile fracture stress. As a result, these materials often fail in tension before they exhibit macroscopic yielding and the yield stress is usually determined in compression.

The yield-stress studies were conducted in the glassy state over a temperature interval of -70 to 155 °C using 1.27 and 0.64 cm diameter cylindrical specimens. The resins were cast in polytetrafluoroethylene tubes mounted in aluminium moulds and were cured using the schedules described elsewhere [1]. After the initial cure stage, the specimen edges were carefully machined to achieve a height-to-diameter ratio of 2:1. The specimens were then post-cured, using the post-cure schedules described previously [1]. The compression tests were conducted between steel plates enclosed in a controlled-environment chamber and mounted on a servohydraulic testing machine. All tests were conducted at initial nominal strain rates of 3.9×10^{-4}–6.7×10^{-4} s^{-1}.

The true compressive stress was calculated using the relation

$$\sigma_{yc} = \frac{P_y(1 - \varepsilon)}{A_o} \quad (1)$$

where P_y is the compressive load, ε is the nominal strain, and A_o is the undeformed cross-sectional area. The intrinsic yield point, corresponding to the maximum on the true stress–nominal strain curve, was chosen as the yield stress of the material [2].

2.3. Fracture energy

The glassy state critical stress intensity factors were measured using a double torsion (DT) specimen geometry [3]. The DT specimen is ideally suited for crack-propagation studies in brittle materials because the stress intensity factor is independent of the crack length and, if failure occurs in an unstable mode, several crack initiation and arrest studies can be conducted using a single specimen. Under plane strain conditions, the Mode I stress intensity factor, K_{Ic}, is given by

$$K_{Ic} = P_c w_m \left[\frac{1}{wh^3 h_n k_1 (1 - \nu)}\right]^{0.5} \quad (2)$$

where P_c is the critical load at failure, w_m is the moment arm, w is the sample width, h is the sample thickness, h_n is the thickness in the plane of the crack, ν is Poisson's ratio, and k_1 is a constant which depends on the ratio $(w/2h)$. The variation in k_1 with $(w/2h)$ has been tabulated by Young and Beaumont [4] and appropriate values of k_1 were chosen for each specimen according to the $(w/2h)$ ratio.

Rectangular specimens with dimensions of 3.81 cm × 8.9 cm were machined from the cured sheets. The specimen thicknesses varied from 0.25–0.46 cm for different batches of cured sheets. The specimens were notched at one end and a V-shaped groove with a depth of about one-tenth the specimen thickness was milled along one face of the specimen length. After machining, the specimens were post-cured according to the schedules described earlier [1]. A starter crack was then inserted into the post-cured specimens by gently tapping a fresh blade into the notch until the crack grew a distance of 5–10 mm ahead of the notch. For each network, at least three and up to five specimens were tested at each temperature.

The fracture tests were conducted at a loading rate of 0.05 cm min^{-1} over a temperature interval of -70 to 135 °C. Sub-ambient temperatures were achieved by controlled evaporation of liquid nitrogen into the environmental chamber and the temperature was regulated to within ± 2 °C using electric heaters.

Plane strain conditions were verified for each measurement using the plane strain thickness criterion [2, 5]

$$h_n \geqslant 2.5\left(\frac{K_{Ic}}{\sigma_{yt}}\right)^2 \quad (3)$$

where σ_{yt} is the tensile yield stress. Values of σ_{yt} were estimated as 0.75 σ_{yc}, where σ_{yc} is the experimentally determined compressive yield stress, as suggested by Kinloch *et al.* [6]. The fracture energy under plane strain conditions was calculated using the relation

$$G_{Ic} = \frac{K_{Ic}^2(1-\nu^2)}{E} \quad (4)$$

where E is the tensile modulus, results for which were reported earlier [1]. For unstable crack growth, the critical stress intensity factors for crack initiation, K_{Ici}, and crack arrest, K_{Ica}, were calculated from Equation 2 using the corresponding values of the load at crack initiation or arrest. The fracture energies for initiation, G_{Ici}, and arrest, G_{Ica}, were then calculated from Equation 4 using the appropriate K_{Ic} values.

2.4. Dynamic effects in unstable crack growth

The fracture properties during the transient stage between crack initiation and arrest are described in terms of dynamic stress intensity factors, K_I^{dyn}, or the dynamic fracture energies, G_I^{dyn}. K_I^{dyn} values are often observed to be a function of crack velocity and are usually greater than the corresponding stress intensity factors for a stationary crack, K_{Ica} [7–10]. Experimental studies with low molecular weight epoxy resins have shown that at the instant of crack arrest, K_I^{dyn} is greater than K_{Ica}, the critical stress intensity factor calculated using a static analysis (Equation 2) [8–10]. However, the dynamic effects decay within 0.5–2 ms after crack arrest and during this time period, K_I^{dyn} also decays to K_{Ica}.

For all the tests in this study, the critical stress intensity factors at arrest were calculated assuming a stationary crack. The data acquisition for the fracture tests was performed at a sampling rate of 1 Hz, i.e. the time interval between successive load measurements was 1 s. Thus, although dynamic effects were not measured, a sufficient time interval was permitted between successive load measurements to allow the dynamic effects to dissipate after crack arrest and before a subsequent load measurement.

2.5. Fractography

The fracture surfaces of representative DT specimens were studied with optical and scanning electron microscopes (SEM). Samples for optical microscopy were examined without any prior treatment, while samples for SEM studies were sputter-coated with a thin film of platinum–gold. The optical micrographs were obtained using a Reichert Model 300/928 microscope at a magnification of × 73. The SEM studies were conducted with an ETEC–Autoscan SEM at an excitation voltage of 20 ke V and at magnifications of × 200 and × 500.

3. Results and discussion

3.1. Yield stress

The results of the yield-stress studies are presented in Fig. 2. For the temperature interval and the range of $\bar{M}_c$ values studied, the yield stress decreased linearly with an increase in temperature. At all temperatures, the most densely cross-linked network, Epon 825/*m*PDA, exhibited the highest yield stress. The magnitude of the yield stress decreased with

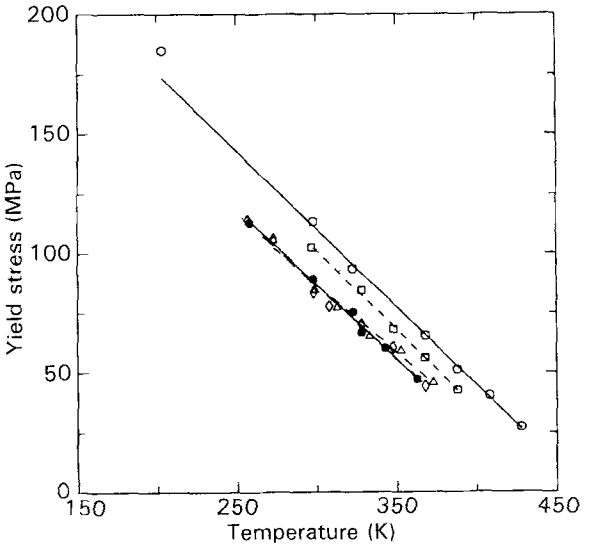

Figure 2 Temperature dependence of the true compressive yield stress of a series of Epon resins cured with *m*PDA, (○) Epon 825/*m*PDA, (□) Epon 836/*m*PDA, (△) Epon 1001F/*m*PDA, (◇) Epon 1002F/*m*PDA, (●) Epon 1004F/*m*PDA.

an increase in the molecular weight between cross-links up to about 775 g mol^{-1} corresponding to Epon 1001F/*m*PDA. For $\bar{M}_c$ values greater than 775 g mol^{-1}, the yield stress did not vary appreciably with the network cross-link density.

The temperature and the strain-rate dependence of the yield behaviour of polymers have been modelled using the Eyring theory of viscosity [11, 12]. For temperatures below the glass transition temperature, but above the secondary or the β-transition temperature of the polymer, the expression for the yield stress is

$$\frac{|\sigma_y|}{T} = \frac{R}{v^*} \sinh^{-1}\left[\frac{\dot{\varepsilon}}{2A_E} \exp\left(\frac{\Delta E^*}{RT}\right)\right] \quad (5)$$

where σ_y is the yield stress, $\dot{\varepsilon}$ is the strain rate, and A_E is a material constant. At the high stresses typically encountered at yield in glassy polymers, Equation 5 can be approximated, assuming $\sinh x \simeq \exp(x)/2$ (i.e. for large x) as,

$$\frac{|\sigma_y|}{T} = \frac{\Delta E^*}{v^* T} + \frac{R}{v^*} \ln\left(\frac{\dot{\varepsilon}}{A_E}\right) \quad (6)$$

ΔE^* in the above equations is a measure of the activation energy, i.e. the energy required by the segments of the polymer backbone chain under the influence of yield stress and thermal energy to jump from one equilibrium position to another, and v^* is the volume of a polymer segment involved in the yield process.

For a given material, i.e. constant A_E, and for tests conducted at constant strain rates, the Eyring model predicts a linear relationship between yield stress and temperature. The results in Fig. 2 confirm the linear behaviour for the networks of this study. The slopes and the intercepts of the yield stress–temperature plots for the five networks are listed in Table III. Because the backbone structure of the resin for all the networks is the same, and because the tests were conducted at similar strain rates, the ratio $(\dot{\varepsilon}/A_E)$ is constant for all the networks. A similarity in the slopes of the σ_y versus temperature plot then indicates that the activation volumes for the networks may be similar.

The magnitudes of the intercepts of the yield stress–temperature plots decrease with increasing $\bar{M}_c$ from Epon 825/*m*PDA to Epon 1001F/*m*PDA. However for $\bar{M}_c$ values greater than about 775 g mol^{-1} (Epon 1001F/*m*PDA) the changes are not appreciable. The changes in the intercepts are the result of the differences in the activation energies involved in the yield process. In order to obtain explicit network structure dependence of ΔE^* and v^*, it is necessary to determine the strain-rate dependence of the yield stress at constant temperature. Because these studies were not undertaken, the influence of cross-link density on the activation energies and volume could not be determined.

TABLE III Parameters describing the temperature dependence of the yield stress (Equation 6)

Network	Slope $\frac{R}{v^*}\ln\left(\frac{\dot{\varepsilon}}{A_E}\right)$ (MPa K^{-1})	Intercept $\left(\frac{\Delta E^*}{v^*}\right)$ (MPa)
Epon 825/*m*PDA	− 0.653	306.2
Epon 836/*m*PDA	− 0.662	299.6
Epon 1001F/*m*PDA	− 0.568	257.4
Epon 1002F/*m*PDA	− 0.610	269.6
Epon 1004F/*m*PDA	− 0.628	275.5

3.2. Fracture properties

The plane strain thickness criterion, defined by Equation 3, was verified for all fracture tests. Except for Epon 825/*m*PDA specimens tested at 135 and 145 °C, and Epon 836/*m*PDA specimens tested at 75 °C, the plane strain thickness criterion was satisfied by all other samples at all test conditions.

The temperature dependence of the fracture energies of the networks is shown in Figs 3–7. The fracture tests were conducted from − 70 to 40 °C below the glass transition temperatures of the respective networks. The fracture energies were calculated from the

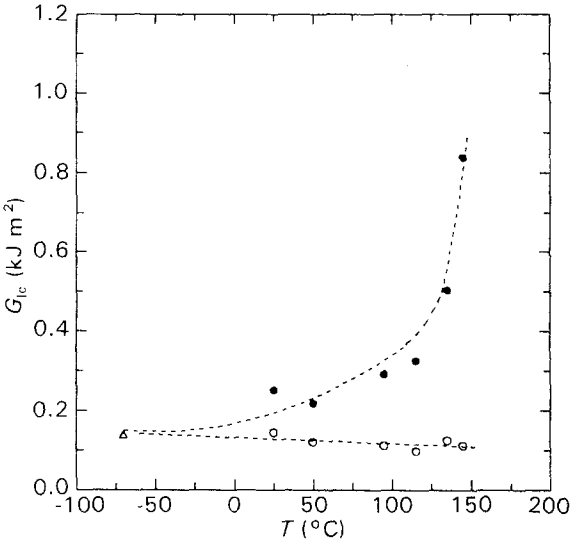

Figure 3 Temperature dependence of fracture energy of Epon 825/*m*PDA. (●) Initiation, (○) arrest, (△) stable.

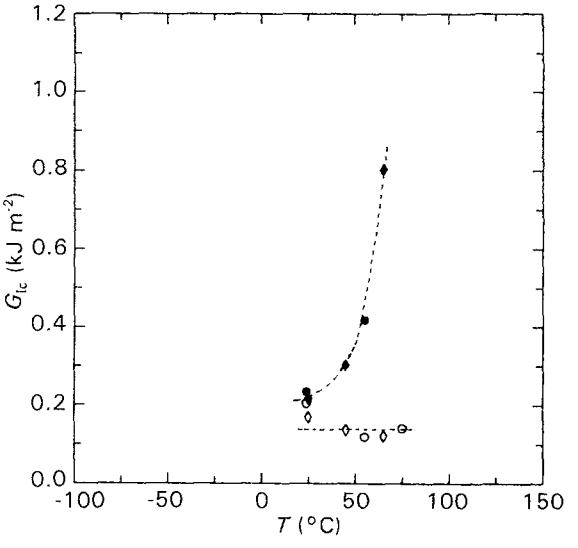

Figure 4 Temperature dependence of fracture energy of (●, ○) Epon 836/*m*PDA and (◆, ◇) Blend (836)/*m*PDA. (●, ◆) Initiation, (○, ◇) arrest.

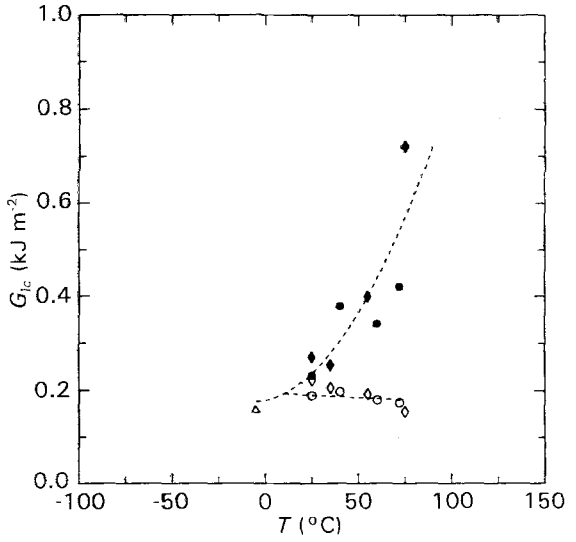

Figure 5 Temperature dependence of fracture energy of (●, ○) Epon 1001F/*m*PDA and (◆, ◇) Blend (1001)/*m*PDA. (●, ◆) Initiation, (○, ◇) arrest, (△) stable (1001F).

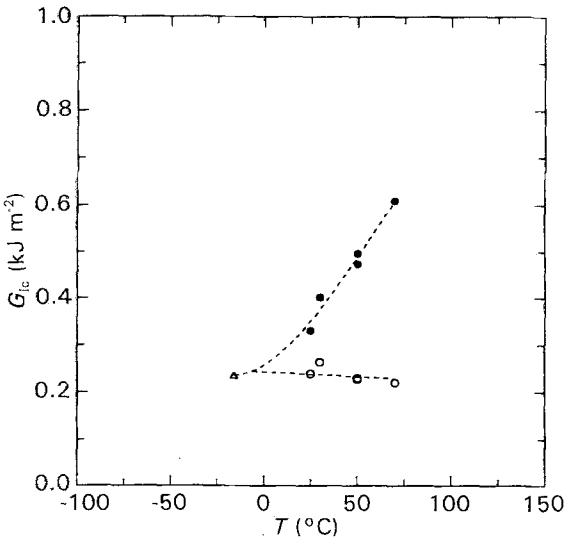

Figure 7 Temperature dependence of fracture energy of Epon 1004F/*m*PDA. (●) Initiation, (○) arrest, (△) stable.

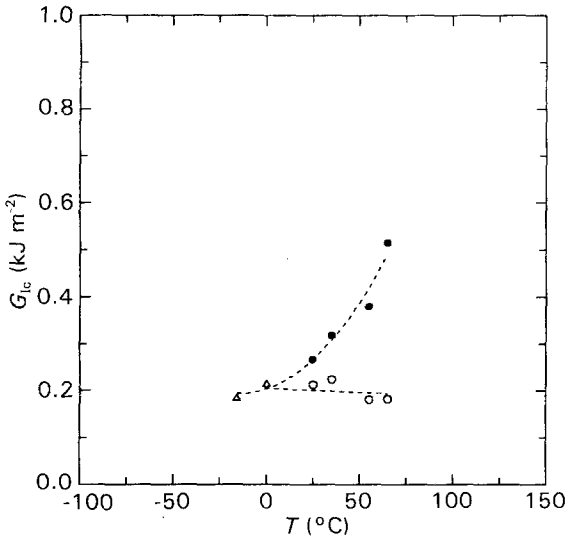

Figure 6 Temperature dependence of fracture energy of Epon 1002F/*m*PDA. (●) Initiation, (○) arrest, (△) stable.

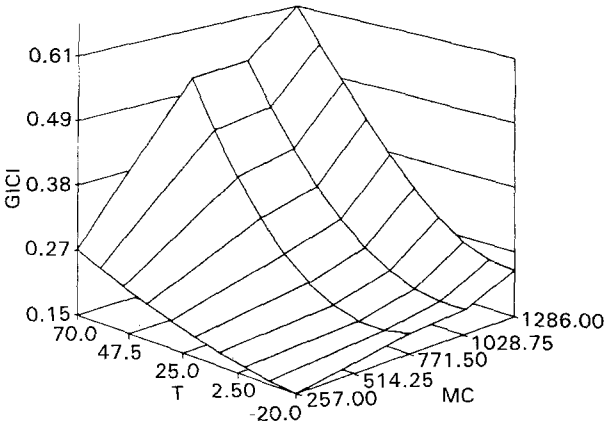

Figure 8 Temperature and molecular weight dependence of the fracture initiation energy of the Epon networks. T = temperature (°C), MC = molecular weight between cross-links (g mol^{-1}), GICI = fracture initiation energy, (kJ m^{-2}).

critical stress intensity factors and the moduli using Equation 4 with the Poisson's ratio, ν, assumed equal to 0.35 [13].

For all the networks, crack propagation occurred in an unstable or "stick–slip" mode above 0 °C, while a stable, continuous mode of failure was observed below 0 °C. When fracture occurred in an unstable manner, the fracture energies for crack initiation, G_{Ici}, increased with increasing temperatures. In contrast, the fracture energies for crack arrest, G_{Ica}, were, within the limits of experimental error, independent of temperature. For Blend (836) and Blend (1001), the temperature dependence of fracture energies was similar to that of Epon 836 and Epon 1001F, respectively, as shown in Figs 4 and 5. This suggests that the fracture properties are not very sensitive to the molecular weight distribution of the epoxy resin.

Using linear or higher-order polynomial fits to the experimental fracture energy results, two-dimensional surfaces were generated to illustrate the molecular weight and temperature dependence of the fracture initiation and arrest energies. The surfaces are shown in Figs 8 and 9. As seen from Fig. 8, G_{Ici} increases both with an increase in temperature and $\bar{M}_c$. In contrast to G_{Ici}, the G_{Ica} values do not exhibit a significant temperature dependence (cf. Fig. 9).

Although a macroscopic linear stress–strain behaviour was observed for the fracture tests, failure is very often preceded by localized crack tip plastic deformations [14]. The temperature dependence of the fracture initiation energy is the result of the temperature dependence of the yield stress. Because the yield stress decreases with increasing temperature, localized yielding occurs more readily at higher temperatures. Considerable energy is dissipated in the localized plastic deformations and thus fracture energy for crack initiation increases with an increase in temperature.

When the test temperature is reduced, the yield stress increases and the extent of localized yielding which can precede fracture is also reduced. Thus, the fracture initiation energy decreases. If the test temperature is reduced far below the glass transition temperature of the network, very little viscous dissipation occurs at the crack tip and the failure mode is of stable

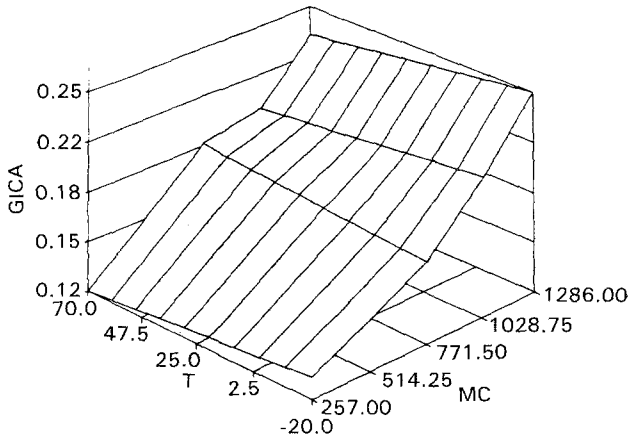

Figure 9 Temperature and molecular weight dependence of the fracture arrest energy of the Epon networks. T = temperature (° C), MC = molecular weight between cross-links (g mol^{-1}), GICA = fracture arrest energy (kJ m^{-2}).

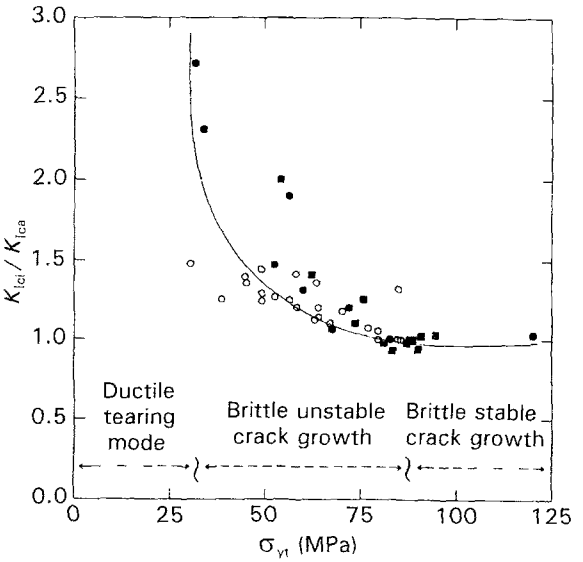

Figure 10 Correlation between K_{Ici}/K_{Ica} and true tensile yield stress, (●) Kinloch and Williams [21], (■) Yamini and Young [13]; (○) present work.

brittle type. Evidence relating the influence of localized plastic deformations on macroscopic fracture initiation energy can be obtained from a study of the fractured specimen surfaces. Analysis of the fractographs is described later.

The relationship between the magnitude of fracture toughness, the yield stress, and the nature of crack propagation can be expressed in the form of a plot of K_{Ici}/K_{Ica} versus σ_{yt}. The variation in K_{Ici}/K_{Ica} versus σ_{yt} for the networks of this study, together with some of the results published earlier, is shown in Fig. 10. For resins with yield stresses of 30–90 MPa, K_{Ici}/K_{Ica} values lie between 1.0 and 1.5 and the crack-growth behaviour is of unstable brittle type. If the yield stresses are greater than 110–120 MPa, very little localized deformation occurs during fracture; K_{Ici} is nearly equal to K_{Ica}, and the crack grows in a stable brittle manner; whereas, for resins with σ_{yt} values lower than 25–30 MPa, K_{Ici}/K_{Ica} is high and crack growth occurs in a ductile stable manner. Over most of the temperature interval investigated in this study, the yield stresses of the Epon networks were such that crack growth occurred in an unstable brittle mode. For tests conducted at temperatures below 0°C, the yield stresses were higher and the mode of crack growth changed to a brittle stable type.

The results in Figs 8 and 9 indicate that at a constant temperature, both the fracture energies for crack initiation and arrest increase with an increase in the average molecular weight between cross-links. While the fracture energies for crack initiation are temperature dependent, the fracture energies for crack arrest are, within the limits of experimental error, independent of temperature. G_{Ica} values have been reported to be independent of strain rate and temperature in other studies [7, 14–16]. Because G_{Ica} does not depend on testing conditions such as temperature, G_{Ica} may be regarded as a material constant, being determined only by the cross-link density of the homologous series of the epoxy/*m*PDA networks.

The variation in the glassy-arrest fracture energies with the molecular weight between cross-links is shown in Fig. 11. The G_{Ica} values shown are the mean

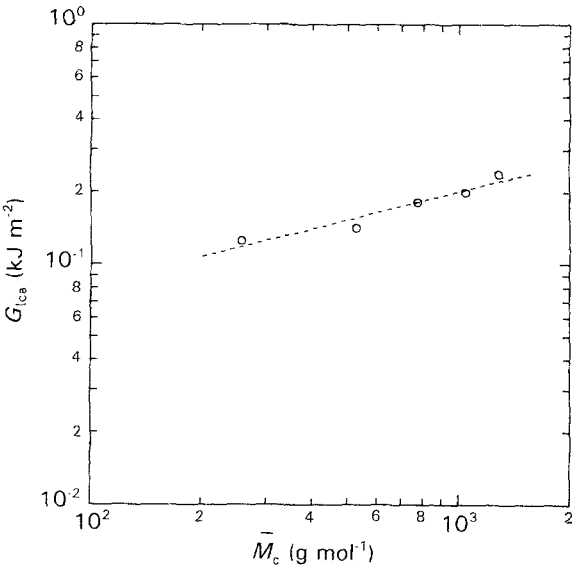

Figure 11 Variation in glassy arrest fracture energies with molecular weight between cross-links for a series of Epon resins cured with *m*PDA.

values for each network, i.e. values averaged over a temperature interval of 0–80 °C to account for the experimental scatter. A linear correlation is observed between $\log(G_{Ica})$ and $\log(\bar{M}_c)$ suggesting a simple power-law relationship of the type

$$G_{Ica} = a_1 \bar{M}_c^{b_1} \quad (8)$$

The least squares fit line through the points has a slope of 0.39 and the proportionality constant, a_1, has a value of 14.02 (J m^{-2}) (g mol^{-1})$^{-0.39}$. A similar relationship has been reported by LeMay and Kelley [16] for a series of epoxy resins cured with diamino diphenylsulphone (DDS). In that case the coefficient b_1 was 0.55 and the constant a_1 was 6.10 (J m^{-2}) (g mol^{-1})$^{-0.55}$. Also, Pearson and Yee [17] have reported fracture energies for DER-332-based epoxies cross-linked with DDS. In their study, Pearson and Yee used single-edge notched specimens and, because fracture occurs in a catastrophic manner for these

samples, only single values of G_{Ic} were reported. For the three networks studied, these investigators also observed a linear relationship between $\log_e(G_{Ic})$ and $\log_e(\bar{M}_c)$ with a slope of 0.30 and a value of a_1 of 26.7 $(J\,m^{-2})\,(g\,mol^{-1})^{-0.30}$.

3.3. Fractographic analysis

In densely cross-linked epoxies, if crack propagation is of stable brittle type, the crack often propagates along a single plane throughout the specimen length and the fracture surfaces are completely featureless. If the crack deviates from the initial plane of propagation due to the presence of dispersed phase heterogeneities or localized plastic deformations, the fracture surface reveals distinct features which characterize the nature of these deformations. When crack grows in an unstable, "stick–slip" manner, the region of the fracture surface representing the slip process, where the crack jumps a short distance at high speeds is completely featureless. The portion of the crack immediately following the crack arrest displays features which are related to the nature of the localized plastic deformations.

A schematic representation of a crack profile and the crack movement in a DT specimen are shown in Fig. 12a. Although the crack front is curved, Evans [3] has shown that for brittle materials failure occurs in the tensile opening mode (Mode I). The fracture surface of a DT specimen formed under typical unstable mode of crack growth is shown in Fig. 12b. The crack arrest line in the figure is the position of the crack at the instant of crack arrest. The coarse region with numerous striations occurs due to the localized plastic deformations prior to a crack jump. The width of this deformation zone is related to the magnitude of localized energy dissipation which occurs before crack initiation; the width is larger for samples with higher G_{Ici} values. The "river markings" or longitudinal lines which run normal to the crack front are possibly the result of secondary cracks which initiate during the slow growth phase. The featureless region before the arrest line and after the coarse region results from brittle fracture with very little plastic deformation when crack growth occurs at high velocities during the "slip" phase.

Micrographs of representative fracture surfaces are shown in Figs 13–19. For Epon 825/*m*PDA tested at 25 °C, the coarse region is relatively narrow in size and the "river markings" are long and grow uniformly from the coarse region. For samples tested at higher temperatures, where the yield stress is relatively lower, the width of the deformation zone is larger, as seen in Figs 15 and 17. Scanning electron micrographs of Epon 825/*m*PDA tested at 25 °C, and 95 °C reveal, in detail, the localized plastic deformations. The extent of deformation is greater at 95 °C than at 25 °C, although the density of the "river markings" is reduced at higher

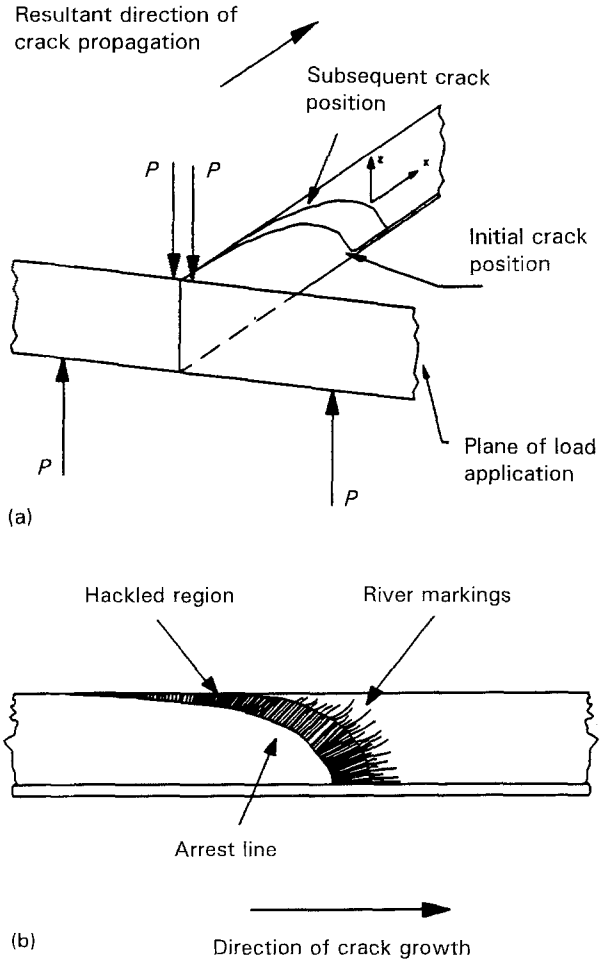

Figure 12(a) Crack profile in a DT specimen. (b) Fracture surface of a DT sample after unstable crack growth.

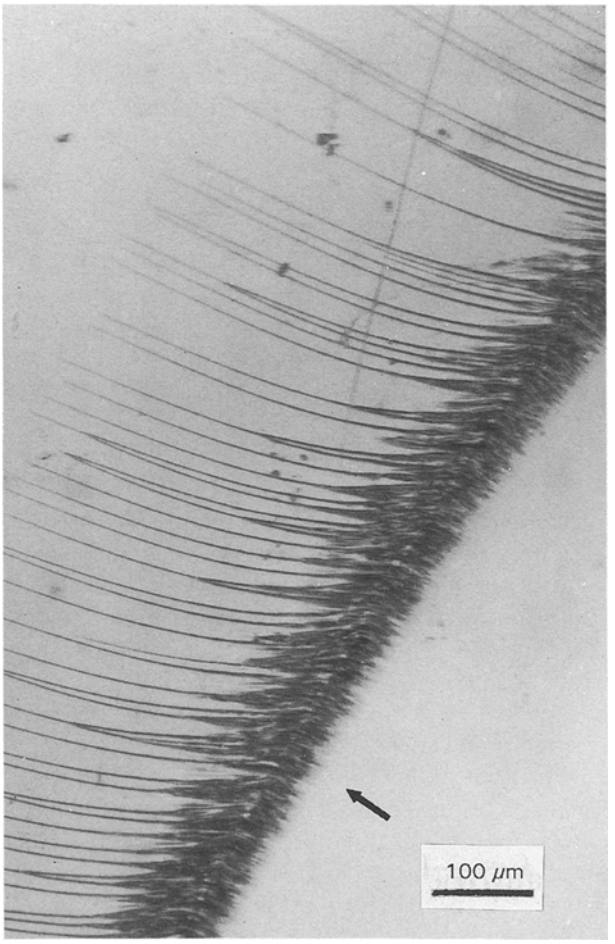

Figure 13 Optical micrograph of Epon 825/*m*PDA tested at 25 °C (the arrow indicates the direction of crack growth).

temperatures. River markings similar to those seen in Figs 13–19 have been reported by a number of investigators from fractographic studies of densely crosslinked epoxies [14, 15, 18–20].

An optical micrograph of an Epon 825/*m*PDA specimen tested at 135 °C and which did not satisfy the plane strain thickness criterion is shown in Fig. 17. This fractograph illustrates plastic deformations which extend beyond the narrow zone observed in samples tested at other temperatures. An enlarged deformation region substantiates the experimentally measured enhancement in fracture energy and a failure to satisfy the plane strain thickness criterion.

Figs 18 and 19 show the optical micrographs of Epon 1002F/*m*PDA and Epon 1004F/*m*PDA. The surface characteristics are very similar to those of Epon 825/*m*PDA with a characteristic coarse deformation zone and an essentially featureless region ahead of and following the deformation zone. The density of the fine "river markings" is lower than for Epon 825/*m*PDA possibly due to fewer secondary cracks; however, the deformation zone appears considerably coarser indicating greater energy dissipation. The width of the deformation zone is largest for Epon 1004F/*m*PDA tested at 70 °C which also exhibits the highest G_{Ici}.

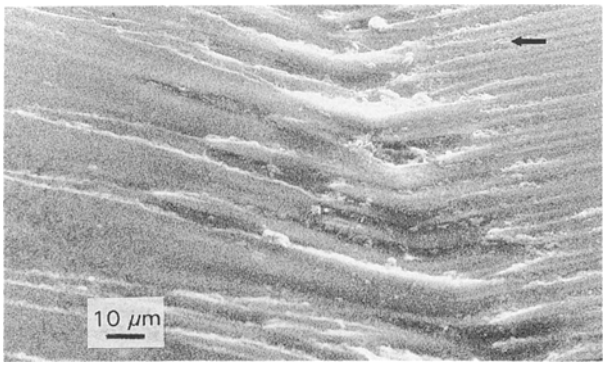

Figure 14 Scanning electron micrograph of Epon 825/*m*PDA tested at 25 °C (the arrow indicates the direction of crack growth).

Figure 16 Scanning electron micrograph of Epon 825/*m*PDA tested at 95 °C (the arrow indicates the direction of crack growth).

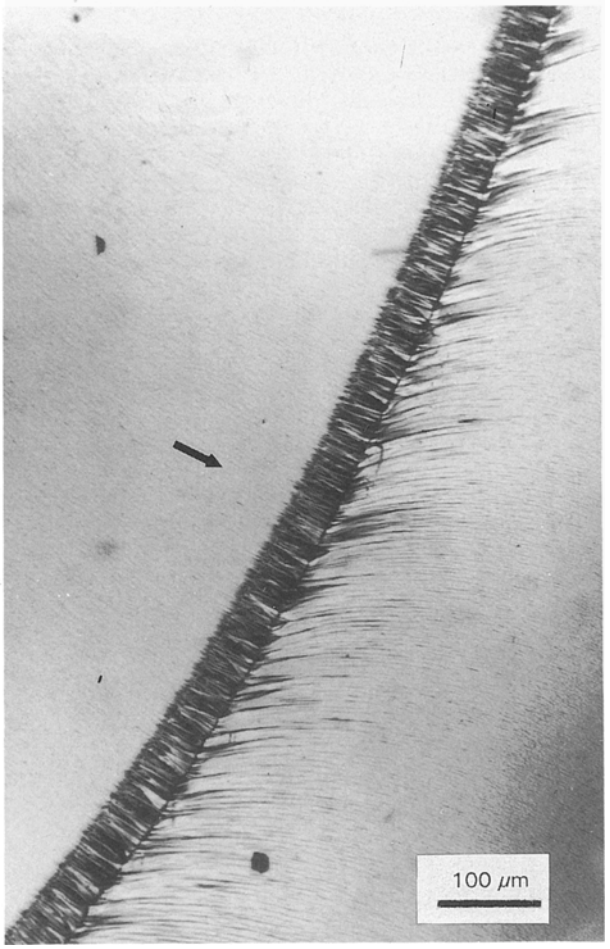

Figure 15 Optical micrograph of Epon 825/*m*PDA tested at 95 °C (the arrow indicates the direction of crack growth).

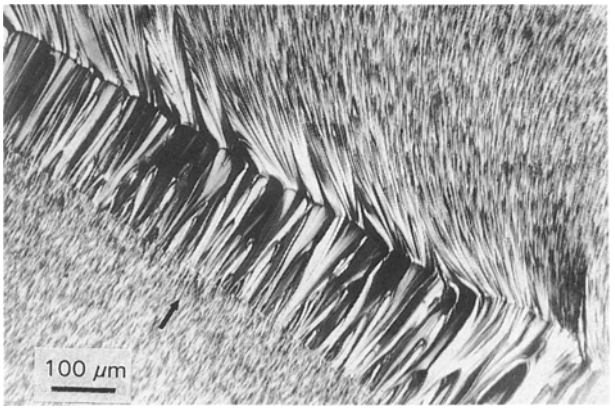

Figure 17 Optical micrograph of Epon 825/*m*PDA tested at 135 °C (the arrow indicates the direction of crack growth).

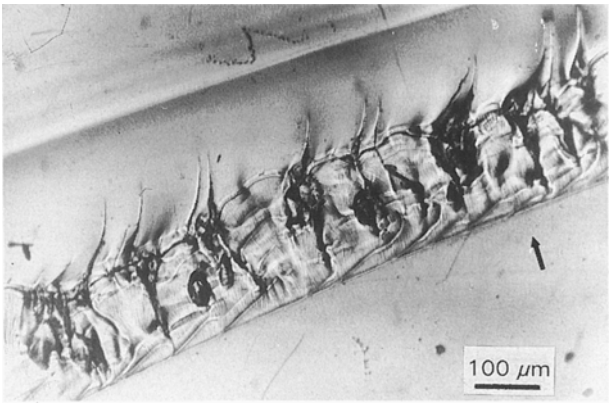

Figure 18 Optical micrograph of Epon 1002F/*m*PDA tested at 50 °C (the arrow indicates the direction of crack growth).

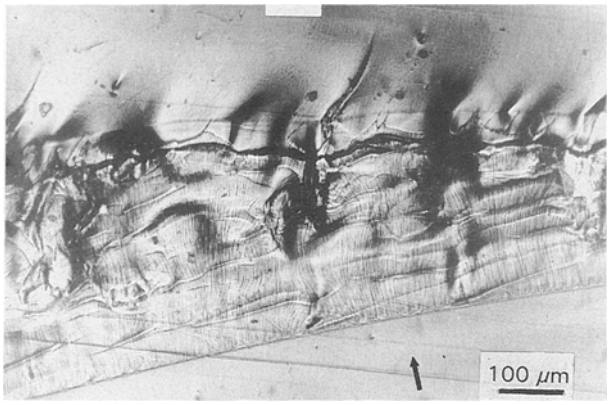

Figure 19 Optical micrograph of Epon 1004F/*m*PDA tested at 70 °C (the arrow indicates the direction of crack growth).

4. Conclusions

The yield and fracture behaviour of a series of epoxy resins were studied to determine the influence of the network structure on mechanical properties. For all the networks, the yield stress was observed to decrease linearly with increasing temperatures; this behaviour was explained by the Eyring theory of viscosity. The slopes of the yield stress–temperature plots for all the networks were similar, possibly due to a similarity in the activation volumes involved in the yield process. An explicit molecular weight dependence of the activation energy for yield could not be determined because the variation in yield stress with strain rate was not studied.

For all the networks, the crack propagation behaviour was observed to change from a stable continuous mode below 0 °C to an unstable, "stick–slip" mode above 0 °C. Unstable crack-growth behaviour was attributed to localized crack-tip yielding. The fracture energies for crack initiation increased with increasing temperatures due to the temperature dependence of the yield stress. The fracture energies for crack arrest were nearly independent of temperature and were similar to the fracture energies for stable crack propagation. The results of this study suggest that the glassy arrest fracture energies may represent a material property. An empirical $G_{Ica} = a_1 \bar{M}_c^{b_1}$ type correlation was observed between the glassy arrest fracture energies and the molecular weight between cross-links.

Fractographs of the DT specimens showed greater deformation zone sizes for samples tested at higher temperatures due to greater localized yielding. For most samples, the fracture surface beyond the narrow deformation zone was featureless resulting from rapid crack propagation along a single plane. However, an Epon 825/*m* PDA sample which failed to satisfy the plane strain thickness criterion showed increased deformations outside the narrow plastic zone, revealing evidence of increased plastic deformation.

Acknowledgement

The authors thank Mr Paul Jones, Shell Development Company, for the generous supply of the Epon resins.

References

1. U. M. VAKIL and G. C. MARTIN, *J. Appl. Polym. Sci.* **46** (1992) 2089.
2. A. J. KINLOCH and R. J. YOUNG, in "Fracture Behavior of Polymers" (Applied Science, London, 1983) Chap. 3.
3. A. G. EVANS, *Int. J. Fract.* **9** (1973) 267.
4. R. J. YOUNG and P. W. R. BEAUMONT, *Polymer* **12** (1977) 684.
5. D. BROEK, in "Elementary Engineering Fracture Mechanics" (Martinus Nijhoff, Dordrecht, 1986).
6. A. J. KINLOCH, S. J. SHAW and D. L. HUNSTON, *Polymer* **24** (1983) 1355.
7. R. A. GLEDHILL and A. J. KINLOCH, *Polym. Eng. Sci.* **19** (1979) 82.
8. J. F. KALTHOFF, S. WINKLER and J. BEINERT, *Int. J. Fract.* **12** (1976) 161.
9. J. F. KALTHOFF, J. BEINERT, and S. WINKLER, in "Fast Fracture and Crack Arrest", edited by G. T. Hahn and M. F. Kanninen, ASTM STP 627 (American Society for Testing and Materials, Philadelphia, PA. 1977).
10. J. F. KALTHOFF, J. BEINERT, S. WINKLER, and W. KLEMM, in "Crack Arrest Methodology and Applications", edited by G. T. Hahn and M. F. Kanninen, ASTM STP 711 (American Society for Testing and Materials, Philadelphia, 1980).
11. H. EYRING, *J. Chem. Phys.* **4** (1936) 283.
12. C. BAUWENS-CROWET, J-C. BAUWENS and G. J. HOMÈS, *J. Mater. Sci.* **7** (1972) 176.
13. S. YAMINI and R. J. YOUNG, *Polymer* **18** (1977) 1075.
14. D. C. PHILLIPS, J. M. SCOTT and M. JONES, *J. Mater. Sci.* **13** (1978) 311.
15. J. M. SCOTT, G. M. WELLS and D. C. PHILLIPS, *J. Mater. Sci.* **15** (1980) 1436.
16. J. D. LeMAY and F. N. KELLEY, *Adv. Polym. Sci.* **78** (1986) 115.
17. R. A. PEARSON and A. F. YEE, *Am. Chem. Soc. Proc. Div. Polym. Mater. Sci. Eng.* **49** (1983) 316.
18. S. YAMINI and R. J. YOUNG, *J. Mater. Sci.* **15** (1980) 1823.
19. A. C. MOLONEY and H. H. KAUSCH, *J. Mater. Sci. Lett.* **4** (1985) 289.
20. H. H. KAUSCH, in "Polymer Fracture" (Springer, Berlin, 1987).
21. A. J. KINLOCH and J. G. WILLIAMS, *J. Mater. Sci.* **15** (1980) 987.

Received 14 April 1992
and accepted 24 February 1993